



Climate Projections over the Great Lakes Region: Using Two-way Coupling of a Regional Climate Model with a 3-D Lake Model

Pengfei Xue^{1,2,6,7,*}, Xinyu Ye^{1,2}, Jeremy S. Pal^{3,4}, Philip Y. Chu⁵, Miraj B. Kayastha¹, and Chenfu Huang²

¹Department of Civil, Environmental and Geospatial Engineering, Michigan Technological University, Houghton, MI

²Great Lakes Research Center, Michigan Technological University, Houghton, MI

³Department of Civil Engineering and Environmental Science, Loyola Marymount University, Los Angeles, California

⁴Risk Assessment and Adaptation Strategies Division, Euro-Mediterranean Center on Climate Change and Ca' Foscari University, Venice, Italy

⁵NOAA/Great Lakes Environmental Research Laboratory, Ann Arbor, Michigan

⁶Environmental Science Division, Argonne National Laboratory, Lemont, IL

⁷Department of Civil and Environmental Engineering, Massachusetts Institute of Technology, Cambridge, MA

Corresponding Author: Pengfei Xue (pexue@mtu.edu)

1 Abstract

2 Warming trends of the Laurentian Great Lakes and surrounding areas have been observed in recent
3 decades, and concerns continue to rise about the pace and pattern of future climate change over the
4 worlds largest freshwater system. To date, many regional climate models used for the Great Lakes
5 projection either neglected the lake-atmosphere interactions or only coupled with 1-D column
6 lake models to represent the lake hydrodynamics. The study presents the Great Lakes climate
7 change projection that has employed the two-way coupling of a regional climate model with a 3-D
8 lake model (GLARM) to resolve 3-D hydrodynamics important for large lakes. Using the three
9 carefully selected CMIP5 AOGCMS, we show that the GLARM ensemble average substantially
10 reduces the surface air temperature and precipitation biases of the driving AOGCM ensemble
11 average in present-day climate simulations. The improvements are not only displayed from the
12 atmospheric perspective but also evidenced in accurate simulations of lake temperature, and ice



13 coverage and duration. After that, we present the GLARM projected climate change for the
14 mid-21st century (2030-2049) and the late century (2080-2099) for the RCP 4.5 and RCP 8.5.
15 Under RCP 8.5, the Great Lakes basin is projected to warm by 1.3-2.2°C by the mid-21st century
16 and 4.0-4.9°C by the end of the century relative to the early-century (2000-2019). Moderate
17 mitigation (RCP 4.5) reduces the mid-century warming to 0.8-1.9°C and late-century warming
18 to 1.8-2.7°C. Annual precipitation in GLARM is projected to increase for the entire basin, varying
19 from -0.4% to 10.5% during the mid-century and 1.2% to 28.5% during the late-century under
20 different scenarios and simulations. The most significant increases are projected in spring and
21 early summer when current precipitation is highest and little increase in winter when it is lowest.
22 Lake surface temperatures (LSTs) are also projected to increase across the five lakes in all of the
23 simulations, but with strong seasonal and spatial variability. The most significant LST increase
24 will occur in Lake Superior. The strongest warming was projected in spring, followed by strong
25 summer warming, suggesting earlier and more intense stratification in the future. In contrast, a
26 relatively smaller increase in LSTs during fall and winter are projected with heat transfer to the
27 deepwater due to strong mixing and energy required for ice melting. Correspondingly, the highest
28 monthly mean ice cover is projected to be 3-6% and 8-20% across the lakes by the end of the
29 century in RCP 8.5 and RCP 4.5, respectively. In the coastal regions, ice duration will decrease by
30 up to 30-50 days.

31 **Keywords:** Two-way Coupling; Climate Change; Climate Projection; Great Lakes; Earth System;
32 Model Development

33 1 Introduction

34 The Laurentian Great Lakes are the world's largest surface freshwater systems, containing 84%
35 of North America's surface freshwater and 21% of the world's supply of surface fresh water (EPA
36 2014). Spanning more than 244,000 km², an area roughly equal to the size of the United Kingdom,
37 the vast inland freshwater system provides water for consumption, transportation, power, recreation,
38 and many other uses. The Great Lakes support 1.3 million jobs and \$82 billion in wages per year
39 (Rau et al. 2020). More than 34 million people call the Great Lakes basin home, and more than
40 3500 species of plants and animals inhabit it, including over 170 species of fish (EPA 2014). The
41 Great Lakes commercial, recreational, and tribal fisheries are collectively valued at more than
42 \$7 billion annually and support more than 75,000 jobs ([http://www.glfc.org/the-fishery.
43 php](http://www.glfc.org/the-fishery.php)).

44 In recent decades, Great Lakes and surrounding areas have undergone rapid warming (Austin and
45 Colman 2007; Dobiesz and Lester 2009; Hayhoe et al. 2010; Melillo et al. 2014; Pryor et al. 2014;



46 Zhong et al. 2016). The annual mean temperature over the Great Lakes basin has increased by
47 0.9°C between 1901-1960 and 1985-2016, exceeding average changes of 0.7°C for the rest of the
48 contiguous United States (Wuebbles et al. 2019). Consequently, lake surface temperature (LST)
49 in the Great Lakes has increased and ice coverage has decreased. Summer LST has risen faster
50 than the ambient air temperature in Lake Superior (Austin and Colman 2008; McCormick and
51 Fahnenstiel 1999). Ice coverage has reduced by 71% on the Great Lakes as a whole from 1973
52 through 2010 (Wang et al. 2012).

53 Measurable changes have also been observed in precipitation patterns, lake levels, wave climate,
54 and water biogeochemistry impacting the ecosystems (Huang et al. 2021b; Jones et al. 2006;
55 Wuebbles et al. 2019). For example, climate change and human activities have influenced algal
56 bloom frequency and intensity (Dalolu et al. 2012; Dobiesz and Lester 2009; Scavia et al. 2014)
57 reduced primary productivity (Poesch et al. 2016), and altered prey fish habitats and population
58 (Collingsworth et al. 2017; Lynch et al. 2016; Sharma et al. 2007). As a result, there has been a
59 growing need to better understand climate change and variability for the Great Lakes and surrounding
60 regions.

61 Various techniques have been used to project how the Great Lakes regional climate will evolve in
62 the future. The direct use of coupled Atmosphere-Ocean General Circulation Models (AOGCMs)
63 simulation results has shown various problems due to their typical low spatial resolution resulting
64 in inadequacies in representing small-scale processes important in the region (MacKay and Seglenieks
65 2013). More importantly, many Coupled Model Intercomparison Project Phase 5 (CMIP5) models
66 do not include credible representations of Great Lakes (Briley et al. 2021). Dynamical downscaling
67 using higher-resolution regional climate models (RCMs) has been used to improve on these inadequacies
68 (e.g., Music et al. 2015; Notaro et al. 2015; Xiao et al. 2018; Zhang et al. 2019, 2018, 2020).
69 Statistical downscaling (Byun and Hamlet 2018; Byun et al. 2019) and probabilistic projection
70 using a Bayesian Hierarchical Model (Wang et al. 2017) have also been recently applied to the
71 Great Lakes region.

72 Regardless of the techniques used, temperatures over the Great Lakes basin are predicted to increase
73 with anthropogenic atmospheric greenhouse gasses (GHGs) (e.g., Byun and Hamlet 2018; Cherkauer
74 and Sinha 2010; Zhang et al. 2020). Projected precipitation changes are less certain, however,
75 several studies project reductions in summer precipitation and increases in winter and spring, as
76 well as an increase in the fraction of precipitation falling as rainfall (Byun and Hamlet 2018;
77 Cherkauer and Sinha 2010; Notaro et al. 2015; Zhang et al. 2019). Similarly, the lakes themselves
78 are projected to continue to rapidly warm, resulting in reduced ice cover and earlier occurrence
79 of seasonal stratification (Gula and Peltier 2012; Notaro et al. 2015; Xiao et al. 2018). These
80 changes can further modify the distribution of lake mixing regimes and shift the timing of lake
81 overturning episodes (Woolway and Merchant 2019), and can have profound implications for lake
82 biogeochemistry, ecosystems, power production, navigation, tourism, and other sectors.



83 Uncertainties in Great Lakes climate change projections can arise from multiple sources including
84 GHG emission scenarios, internal variability, model deficiencies and lateral forcing conditions.
85 However, land-lake-ice-atmosphere interactions must be taken into account. While significant
86 improvements have been made in modeling these systems, they are typically modeled independently,
87 loosely coupled, or with only a limited set of interactions. Few previous studies have applied
88 a dynamical approach to downscaling AOGCM for climate change projections with results of
89 changes in Great Lakes conditions (Gula and Peltier 2012; Mailhot et al. 2019; Notaro et al. 2015).
90 However, these studies generally treated the Great Lakes as one-dimensional (1D) water columns
91 and ignored three-dimensional (3D) processes in the large lakes (Bennington et al. 2014; Hostetler
92 et al. 1993; Subin et al. 2012). Incorporating 3D hydrodynamic models into RCMs to represent the
93 hydrodynamics of the Great Lakes has been advocated by the Great Lakes modeling community
94 but still in its early stage (Delaney and Milner 2019). Recently, Xue et al. (2017) developed the first
95 two-way coupled RCM and 3D hydrodynamic model system and demonstrated the feasibility and
96 clear benefit of this approach for regional climate simulation. This approach leads to more accurate
97 representations of surface wind regulated sensible and latent heat fluxes that reduce in LST biases
98 (Xue et al. 2015) and improve the simulation of atmospheric conditions such as precipitation and
99 lake-effect snow due to improved representation of LSTs (Shi and Xue 2019). More recently,
100 a similar study using the Climate-Weather Research and Forecasting Model (CWRf) coupled
101 with FVCOM developed for historical simulations (Sun et al. 2020) also demonstrated improved
102 performance when coupling atmosphere and 3-D lake models in a two-way fashion. These two
103 efforts, however, have focused on model development and validation. To date, no studies exist
104 applying such coupled 3-D two-way coupled models to project evolution of the Great Lakes
105 themselves interacting with regional climate changes.

106 In this study, a RCM two-way coupled with a 3-D hydrodynamic model to fully resolve the
107 lake-ice-atmosphere interactions is utilized to provide more reliable high-resolution projections of
108 climate change for the Great Lakes and surrounding regions. Ensemble projections are conducted
109 for the mid- and late twenty-first century under a "business as usual" Representative Concentration
110 Pathway (RCP) scenario (RCP 8.5) and a mitigation scenario (RCP 4.5). The paper documents the
111 model development, validation, and climate change projections. Emphasis is placed on the climate
112 change over the Great Lakes basin as well as its impacts on and interactions with the changes
113 within the lakes.

114 **2 Model and Numerical Experiment Design**

115 **2.1 GLARM**

116 The Great Lakes Atmosphere Regional Model (GLARM) is a two-way lake-ice-atmosphere coupled
117 climate model designed for the Great Lakes region (Xue et al. 2017). GLARM consists of the
118 4th version of the International Centre for Theoretical Physics (ICTP) Regional Climate Model



119 (RegCM4) to simulate land and atmospheric processes (Giorgi et al. 2012) and the Finite Volume
120 Community Ocean Model (FVCOM) to simulate the 3-D lake dynamics, thermal dynamics, and
121 ice dynamics (Chen et al. 2012). The version of RegCM4 applied in this study is a 3-D, hydrostatic,
122 compressible, primitive equation, σ -coordinate and has a nearly identical configuration to RegCM3
123 (Pal et al. 2007). FVCOM is an unstructured-grid, finite-volume, 3-D, primitive equation, hydrodynamic
124 model with a generalized, terrain-following coordinate system in the vertical and triangular meshes
125 in the horizontal, and is widely applied to coastal oceans and the Great Lakes (Anderson et al. 2018;
126 Huang et al. 2021a, 2019; Ibrahim et al. 2020; Xue et al. 2014, 2020, 2015; Ye et al. 2019, 2020).

127 GLARM has been configured with a large domain and small domain in this study. The large
128 domain includes the majority of North America (NA) to fully enable model internal variability
129 and dynamic consistency (Fig. 1, green box, hereafter referred to GLARM-large). The RegCM4
130 module (land, atmosphere and ocean) has an 18-km horizontal grid spacing and 18 vertical sigma
131 layers. The FVCOM module (Great Lakes) has a horizontal resolution of unstructured triangular
132 grids that varies from 1-2 km near the coast to 2-4 km in the offshore region of the lakes. The
133 model is configured with 40 sigma layers to provide a vertical resolution of < 1 m for nearshore
134 waters and 2-5 m in most of the offshore regions of the lakes. The smaller domain is identical in
135 configuration but limited in coverage to the Midwest and Northeast United States and the Ontario
136 and Quebec Canadian provinces (Fig. 1, red box, hereafter referred to GLARM-small), comparable
137 in size to other previous Great Lakes RCM configurations (e.g., Bennington et al. 2014; Xiao et al.
138 2018). This smaller domain, which may be influenced more by driving AOGCMs through lateral
139 boundary conditions, serves as a computationally efficient alternative to the larger domain for
140 comparison.

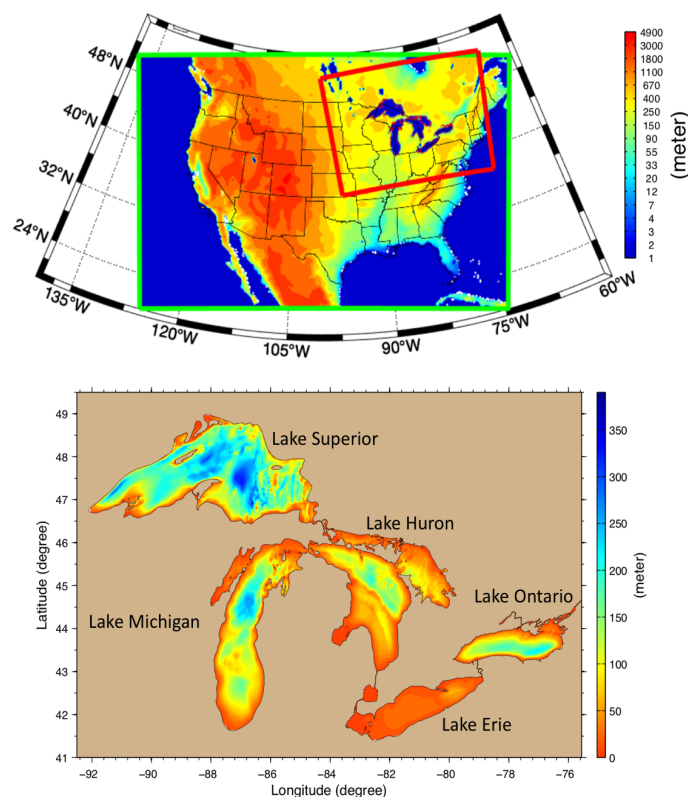


Figure 1: Top: GLARM configured with a large North America domain (green box) and GLARM configured with a smaller domain (red box). Bottom: Bathymetry of the Great Lakes.

141 2.2 Data for Model Validation

142 Various datasets were used in this study for evaluating the model performance in simulating
143 present-day climate, which is a vital step to produce reliable projections. Monthly surface air
144 temperature and precipitation were obtained from the land-station-based 0.5°Climate Research
145 Unit data (CRU TS 3.0) (Harris et al. 2014) and the daily LSTs for the five lakes from the Great
146 Lakes Surface Environmental Analysis (GLSEA; [https://coastwatch.glerl.noaa.gov/glsea/
147 glsea.html](https://coastwatch.glerl.noaa.gov/glsea/glsea.html)). Derived from NOAA/AVHRR (Advanced Very High Resolution Radiometer) satellite
148 imagery, GLSEA serves as the best available product to examine spatial and temporal variability
149 of surface water temperature in the Great Lakes. The daily Great Lakes ice coverage was obtained
150 from the Great Lakes Ice Cover Database (GLICD) using the ice products developed by the
151 U.S. National Ice Center and the Canadian Ice Service (<https://www.glerl.noaa.gov/data/>



152 ice/#historical), which includes the Great Lakes Ice Atlas (<https://www.glerl.noaa.gov/>
153 data/ice/atlas/) for the period 1973-2002 and ice data addendum for 2003 through present.

154 2.3 Numerical Experiment Design

155 The Intergovernmental Panel on Climate Change (IPCC) projections are largely based on AOGCM
156 simulations from the Coupled Model Intercomparison Project (CMIP) coordinated framework.
157 As configured, the output from these simulations is a credible data source for climate change
158 assessments at global, continental, and regional scales; however it may not adequately represent
159 regional and localized features due to the relatively coarse spatial resolution of the AOGCMs (100s
160 km). Using AOGCMs output to drive RCMs has been shown to enhance model performance due
161 largely to a more realistic representation of physics and dynamics as well as orography, coastlines,
162 and land cover as a consequence of their higher resolution. A primary factor of uncertainty
163 associated with the CMIP5 climate change projections is that different AOGCMs can simulate
164 very different climate changes across global, continental and regional scales even under the same
165 anthropogenic forcing scenario. For regional climate modeling studies it is, therefore, critical
166 to evaluate AOGCM performance in the region of interest and select those that best represent
167 climate. In this work, we first evaluate the performance of CMIP5 AOGCMs and then select
168 a subset to use as lateral and ocean surface boundary conditions for GLARM. The GLARM
169 present-day (2000-2019) simulations, driven by the selected AOGCMs, are then validated against
170 observational data. As the CMIP5 AOGCM hindcast simulations ended in 2005, the AOGCM
171 results for 2006-2019 under RCP8.5 were used to drive GLARM for the best track of observed
172 GHG emission (Schwalm et al. 2020). After that, the GLARM projected climate change for
173 the mid-21st century (2030-2049) and the end of the century (2080-2099) for the RCP 4.5 and
174 RCP 8.5 scenarios are presented and discussed. RCP 8.5 is representative of a scenario with
175 high atmospheric GHG concentrations while RCP 4.5 represents a scenario with considerable
176 mitigation.

177 The output from 19 CMIP5 AOGCMs (Table 1) are assessed based on two general reliability
178 criteria (Giorgi and Mearns 2002). The first criteria is based on the ability of the AOGCMs to
179 reproduce different aspects of historical climate, referred to as the "model performance" criterion.
180 The second, referred to as the "model convergence" criterion, assesses the convergence of climate
181 projections by different models under a given forcing scenario. Higher convergence implies more
182 robust signals (Giorgi and Mearns 2002). The reliability score R_k represents the $K_i h$ model performance
183 in simulating the historical climate and its degree of convergence in the projected future climate:

$$R_k = [(R_{B,K})^m \times (R_{D,K})^n] \frac{1}{m \times n} = [(\frac{\epsilon}{|B_k|})^m \times (\frac{\epsilon}{|D_k|})^n] \frac{1}{m \times n}, \quad (1)$$



184

$$\bar{T} = \frac{\sum_{k=1}^n (R_k \times T_k)}{\sum_{k=1}^n R_k} \quad (2)$$

185 $R_{B,k}$ is a factor that is inversely proportional to the absolute bias B_k in simulating the historical
186 variable and $R_{D,k}$ measures the model convergence in terms of the distance (D_k) of the departure
187 of a given model from the average ensemble change weighted by the reliability score of each
188 model R_k (i.e., reliability ensemble average or REA). The parameters m and n (typically equal
189 to 1) represent the weights of the model performance criterion ($R_{B,k}$) and the model convergence
190 criterion ($R_{D,k}$) that influence the reliability score R_k of the model, respectively. The parameter
191 ε describes the natural variability of the climatic variable. \bar{T} is the REA of an assessed variable
192 (e.g. surface air temperature) based on individual value T_k ($k = 1, 19$). The reliability score R_k is
193 calculated iteratively to converge, since R_k is a function of REA, and REA in turn is updated with
194 R_k .

195 To evaluate the performance of each AOGCM in reproducing observed climate and projecting the
196 future warming trend over NA, the model reliability analysis is conducted using model-simulated
197 NA-averaged temperature in the historical periods (1901-2005) and the future period (2006-2100)
198 in RCP 8.5 scenario. The three AOGCMs with the highest reliability scores are selected to drive
199 GLARM for the present-day and two future periods under each scenario.



Table 1: AOGCMs used for reliability analysis.

	GCM Model	Institute	Resolution (degree)	
			Latitude	Longitude
1	ACCESS1.3	Commonwealth Scientific and Industrial Research Organization/Bureau of Meteorology, Australia	1.25	1.875
2	CNRM-CM5	Centre National de Recherches Météorologiques, Centre Européen de Recherche et de Formation Avancée en Calcul Scientifique, France	1.4008	1.40625
3	GFDL-CM3	Geophysical Fluid Dynamics Laboratory, NOAA, United States	2	2.5
4	GFDL-ESM2G	As above	2.0225	2
5	GFDL-ESM2M	As above	2.0225	2.5
6	GISS-E2-H	GISS (Goddard Institute for Space Studies), NASA, United States	2	2.5
7	GISS-E2-R	As above	2	2.5
8	HadGEM2-ES	Met Office Hadley Centre, UK	1.25	1.875
9	IPSL-CM5A-LR	Institut Pierre Simon Laplace, France	1.8947	3.75
10	IPSL-CM5A-MR	As above	1.2676	2.5
11	IPSL-CM5B-LR	As above	1.8947	3.75
12	MIROC5	Atmosphere and Ocean Research Institute, National Institute for Environmental Studies, and Japan Agency for Marine-Earth Science and Technology, Japan	1.4008	1.40625
13	MIROC-ESM-CHEM	As above	2.7906	2.8125
14	MIROC-ESM	As above	2.7906	2.8125
15	MPI-ESM-LR	Max Planck Institute for Meteorology, Germany	1.8653	1.875
16	MPI-ESM-MR	As above	1.8653	1.875
17	MRI-CGCM3	Meteorological Research Institute, Japan	1.12148	1.125
18	NorESM1-M	Bjerknes Centre for Climate Research, Norwegian Meteorological Institute, Norway	1.8947	2.5
19	NorESM1-ME	Bjerknes Centre for Climate Research, Norwegian Meteorological Institute, Norway	1.8947	2.5



200 **3 Results**

201 **3.1 AOGCM Evaluation and Selection**

202 Due to the high computational cost of dynamical downscaling progress using the GLARM, downscaling
203 all AOGCMs is not feasible at this time. Therefore a subset of AOGCMs is selected based on
204 the ability of the AOGCM performance in simulating mean surface air temperature over NA.
205 Among the 19 AOGCMs, the IPSL-CM5A-MR, MPI-ECM-MR, and GISS-E2-H received the
206 highest reliability scores (Table 2). To validate the AOGCM selections, we show that our selected
207 three-model ensemble average (AOGCM-EA3) 1) outperformed 19 individual CMIP5 AOGCMs
208 and 2) was comparable to, if not better than, the 19-model ensemble average (AOGCM-EA19) in
209 three performance metrics including correlation coefficient (R), centered root-mean-square deviation
210 (RMSD) and standard deviation (Std) depicted in the Taylor diagram (Fig. 2-a).

211 These performance metrics are calculated for the 10-year moving average of surface air temperature
212 over NA to evaluate AOGCMs capability of capturing the decadal variation. The scores from the
213 metrics for the 19 AOGCMs span a wide range of values (e.g., R, Std, and RMSD range from
214 0.45-0.93, 0.15-0.45°C and 0.11-0.33°C, respectively). Both AOGCM-EA19 and AOGCM-EA3
215 show very similar performance with a smaller RMSD (0.11-0.12°C) and higher correlation (0.90-0.93)
216 than any single AOGCM; thus highlighting the benefit of ensemble climate modeling. In addition,
217 AOGCM-EA3's standard deviation (0.27°C) is closer to the observation (0.28°C) compared to
218 AOGCM-EA19's (0.21°C), thereby providing us with some confidence in the selected three AOGCMs
219 for dynamical downscaling.

220 In terms of observed warming, the 10-year moving average of annual air temperature for both
221 AOGCM-EA19 and AOGCM-EA3 captures the observed trend, including rapid warming after
222 the 1980s. Additionally, GCM-EA3 tracks the historical temperatures significantly better than
223 GCM-EA19 (Fig. 2-b). The temperatures predicted from GCM-EA3 and GCM-EA19 remain
224 similar to the observations, however after 1930, GCM-EA19 deviates and maintains a nearly
225 constant cold bias of 0.4°C. GCM-EA3, in contrast, closely follows the observation trend and
226 magnitude yielding a mean bias of -0.06°C, which further justifies our selection of the three
227 models.

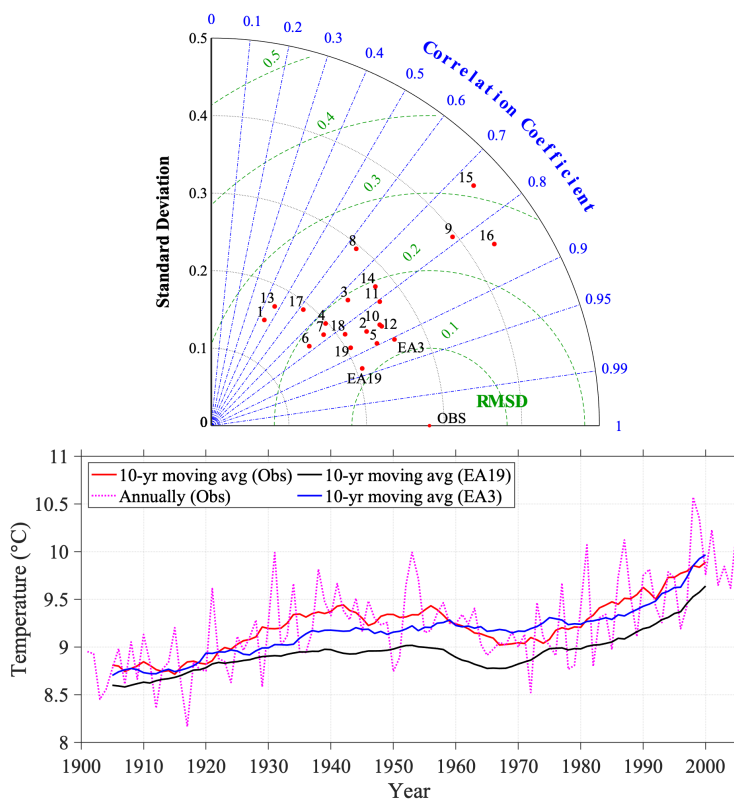


Figure 2: Top: Taylor diagram for 19 individual AOGCMs, ensemble average of 19 AOGCMs (EA19), and ensemble average of the three selected AOGCMs (IPSL-CM5A-MR (10), MPI-ECM-MR (16), and GISS-E2-H (6)) ensemble average (EA3) for the 10-yr moving average of surface air temperature simulation in the period of 1901-2005 over North America. Bottom: Annual surface air temperature (pink), its 10-yr moving average in the period of 1901-2005 comparisons between CRU observations (red), three selected model ensemble average (EA3; blue), and 19-model ensemble average (EA19; black).



Table 2: AOGCMs performance metrics: R, Std, RMSE and model REA score for decadal air temperature simulations over North America in 19 individual AOGCMs and AOGCM-EA19 and AOGCM-EA3.

	GCM Model	Correlation (R)	Standard deviation (Std)	RMSE	REA normalized score
1	ACCESS1-3	0.44	0.15	0.25	0.044
2	CNRM-CM5	0.85	0.23	0.14	0.062
3	GFDL-CM3	0.73	0.23	0.19	0.022
4	GFDL-ESM2G	0.74	0.19	0.18	0.029
5	GFDL-ESM2M	0.89	0.23	0.12	0.042
6	GISS-E2-H	0.77	0.16	0.18	0.113
7	GISS-E2-R	0.77	0.18	0.17	0.059
8	HadGEM2-ES	0.63	0.29	0.24	0.042
9	IPSL-CM5A-LR	0.78	0.39	0.24	0.037
10	IPSL-CM5A-MR	0.85	0.25	0.14	0.119
11	IPSL-CM5B-LR	0.8	0.26	0.17	0.032
12	MIROC5	0.86	0.25	0.14	0.036
13	MIROC-ESM-CHEM	0.46	0.17	0.25	0.013
14	MIROC-ESM	0.76	0.27	0.19	0.013
15	MPI-ESM-LR	0.73	0.45	0.31	0.097
16	MPI-ESM-MR	0.841	0.43	0.24	0.119
17	MRI-CGCM3	0.62	0.19	0.22	0.017
18	NorESM1-M	0.82	0.2	0.16	0.056
19	NorESM1-ME	0.87	0.2	0.14	0.05
20	GCM-EA19	0.93	0.2	0.11	—
21	GCM-EA3	0.9	0.27	0.12	—



228 **3.2 Dynamical Downscaling using GLARM**

229 Before analyzing the climate change projections, we first verify how well GLARM predicts the
230 present-day (2000-2019) surface air temperature, precipitation, lake surface temperature, and ice
231 cover forced by the selected three AOGCMs (IPSL-CM5A-MR, MPI-ECM-MR, and GISS-E2-H)
232 for both GLARM-large and GLARM-small (3 AOGCMs \times 2 domains). The ensemble average of
233 the six-member predictions was hereafter referred to as GLARM-EA6.

234 **3.2.1 Present-day Climate**

235 Figure 3 exhibits GLARM's superiority over the selected three GCMs in reproducing the historical
236 air temperature and precipitation over the Great Lakes basin. Both AOGCM-EA3 and GLARM-EA6
237 reproduce the spatial pattern of observed air temperature well, with the model-data pattern correlations
238 of 0.948 for GLARM-EA6 and 0.987 for AOGCM-EA3 (Fig. 3). However, GLARM-EA6 has a
239 considerably smaller bias (0.18 °C) over the Great Lakes basin compared to AOGCM-EA3 (0.94
240 °C). The warm bias produced by the AOGCM-EA3 for the northern parts of the basin is notably
241 reduced in GLARM-EA6 (Fig. 3-c1,c2). It should be noted that the CRU data inaccurately
242 represents air temperature over the lakes since it is land station based. As all of the selected
243 AOCMs considered ignore or only provide crude representations of the Great Lakes (Fig. 3-b2), the
244 temperature patterns over land and over lake are quite similar. Unlike the GCM-EA3 simulations,
245 GLARM-EA6 simulations indeed manifest the lake influence on the over-lake air temperatures,
246 reinforcing the importance of resolving two-way lake-atmosphere interactions (Fig. 3-b1). The
247 improvement from GLARM-EA6 is also evident with the monthly surface air temperature over
248 land where the bias of AOGCM-EA3 during Jan-Mar and Aug-Oct is nearly zero (Fig. 3-a2). The
249 June and July bias, however, remains in both the AOGCM and GLARM simulations.

250 The added value of the GLARM simulations is also evident in the monthly precipitation. This is
251 clearly reflected in the monthly climatology of the simulated precipitation where GLARM-EA6
252 drastically improved upon the GCM-EA3 monthly precipitation (Fig. 3-d2). The large wet bias
253 during Jan-Aug from the GCM-EA3 is significantly minimized by GLARM-EA6. Compared to
254 GCM-EA3, GLARM-EA6 simulation was closer to the CRU data in nearly every month of the
255 year. The mean bias of GLARM-EA6 is -0.07 mm/day as opposed to GCM-EA3 with 0.35
256 mm/day. Spatially, AOGCM-EA3 displays an abrupt increase in precipitation over the southern
257 portion of the basin (Fig. 3-e2) whereas GLARM-EA6 simulates a gradual latitudinal gradient of
258 precipitation similar to that in the CRU data (Fig. 3-d1, e1), leading to mostly smaller biases over
259 the basin. The wet biases from AOGCM-EA3 near Lake Huron, Erie and Onatrio are noticeably
260 reduced by GLARM-EA6 (Fig. 3-f1, f2).

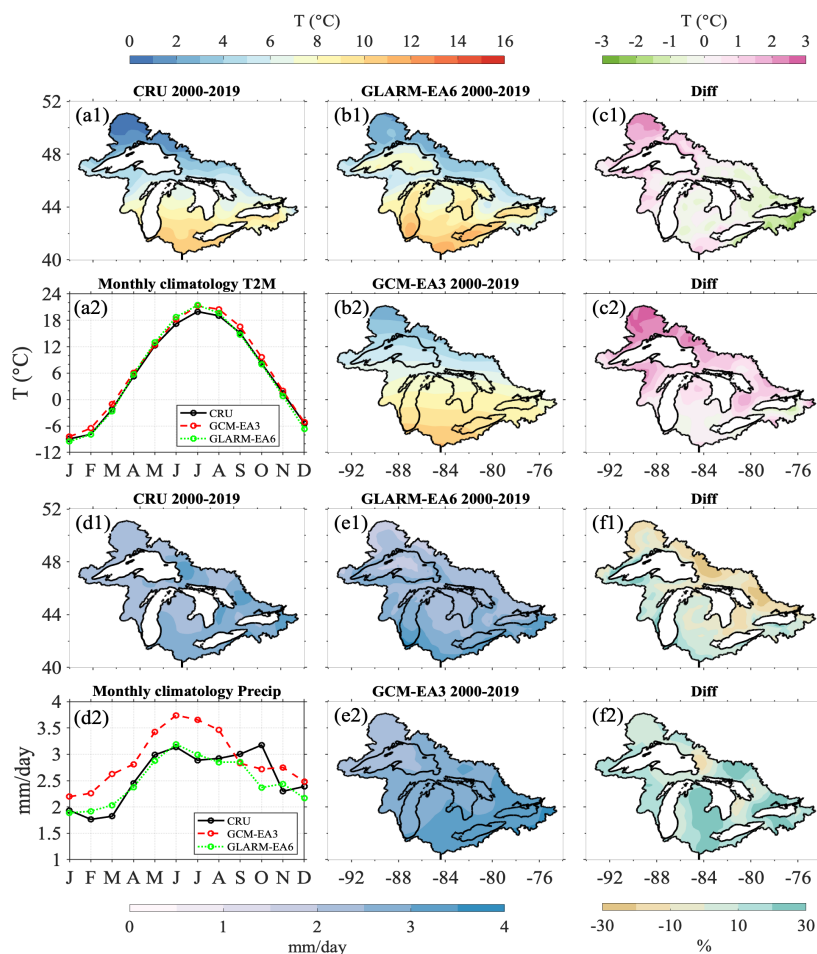


Figure 3: The climatology of surface air temperature and precipitation over the Great Lakes basin (2000-2019) from GLARM-EA6 simulation and GCM-EA3 simulation and their difference (model minus observations) relative to CRU land-based observations. Panels a2 and d2 show the monthly climatology of surface air temperature and precipitation over the land from 2000-2019.

261 Within the Great Lakes, LST and ice cover are the two most important physical lake variables that
 262 influence the lake-atmosphere heat and water fluxes by affecting solar radiation, precipitation, and
 263 evaporation, latent and sensible heat. Since the selected AOGCMs provide little or no representation
 264 of the lakes, they are not included in the analysis. GLARM-EA6 and GLSEA LSTs show close
 265 agreement with each other. LSTs vary significantly across the five lakes due to their immense
 266 surface area, large geographic extent, and varying water depth. This spatial heterogeneity across



267 the lakes is primarily along the meridional direction, resulting in earlier warming in the southern
268 lakes (Fig. 4-a,b,c). Temperature variations are the strongest during summertime when the northernmost,
269 large, deep Lake Superior (average depth 147m) maintains a much cooler temperature of 12-14°C
270 than the temperature of 22-24°C in the southernmost, small, shallow Lake Erie (average depth
271 of 19 m). Additionally, GLARM-EA6 well captures the spatial heterogeneity within each lake.
272 For example, GLARM reproduces the warmer eastern basin of Lake Superior during wintertime,
273 the north-south temperature difference in Lakes Huron-Michigan during summertime, and the
274 east-west thermal gradient in Ontario during fall.

275 In addition to resolving the spatial variability of climatological LST for each of the seasons,
276 GLARM-EA6 performs well in reproducing the GLSEA lake-wide average LSTs (Fig. 5, a1-e1).
277 The GLARM-EA6 predicted LSTs show close agreement with the GLSEA in both phase and
278 magnitude for the five lakes. For example, the spring-early summer warming rate and the summer
279 peaks are well reproduced by GLARM-EA6, which are often not well resolved in previous studies
280 using 1D lake model coupled with RCMs (Bennington et al. 2014; Notaro et al. 2015). While
281 GLARM-EA6 generally closely tracks GLSEA LST across the lakes, relatively large biases are
282 simulated in the warming period in Lake Superior (June, July) and cooling period (October-December)
283 in Lake Erie.

284 Although progress in ice modeling has been made, substantial challenges still remain and as a result
285 larger biases than simulated LSTs typically exist (Anderson et al. 2018; Fujisaki et al. 2013, 2012).
286 GLARM-EA6 captures the spatial variability of ice coverage observed in the GLICD ice data,
287 with higher and lower ice coverage in shallow coastal and deep offshore regions, respectively (Fig.
288 4-e1, e2). GLARM-EA6 predicts ice cover fairly well in Lakes Michigan, Ontario, and Huron;
289 however, it underestimates the magnitude of ice coverage in Lakes Superior and Erie (Fig. 5,
290 a2-e2) although the observed values still fall in the ensemble envelopes. The shallowest lake,
291 Lake Erie, is characterized by the highest ice coverage. GLARM-EA6 underestimates the Lake
292 Erie ice cover by 15%-20% due to the warm biases of the winter LST. For the deepest lake, Lake
293 Superior, GLARM-EA6 does not capture the highest ice coverage observed in March, but instead,
294 it simulates a decrease in ice cover from February to March resulting in an 10% underestimate in
295 ice cover.

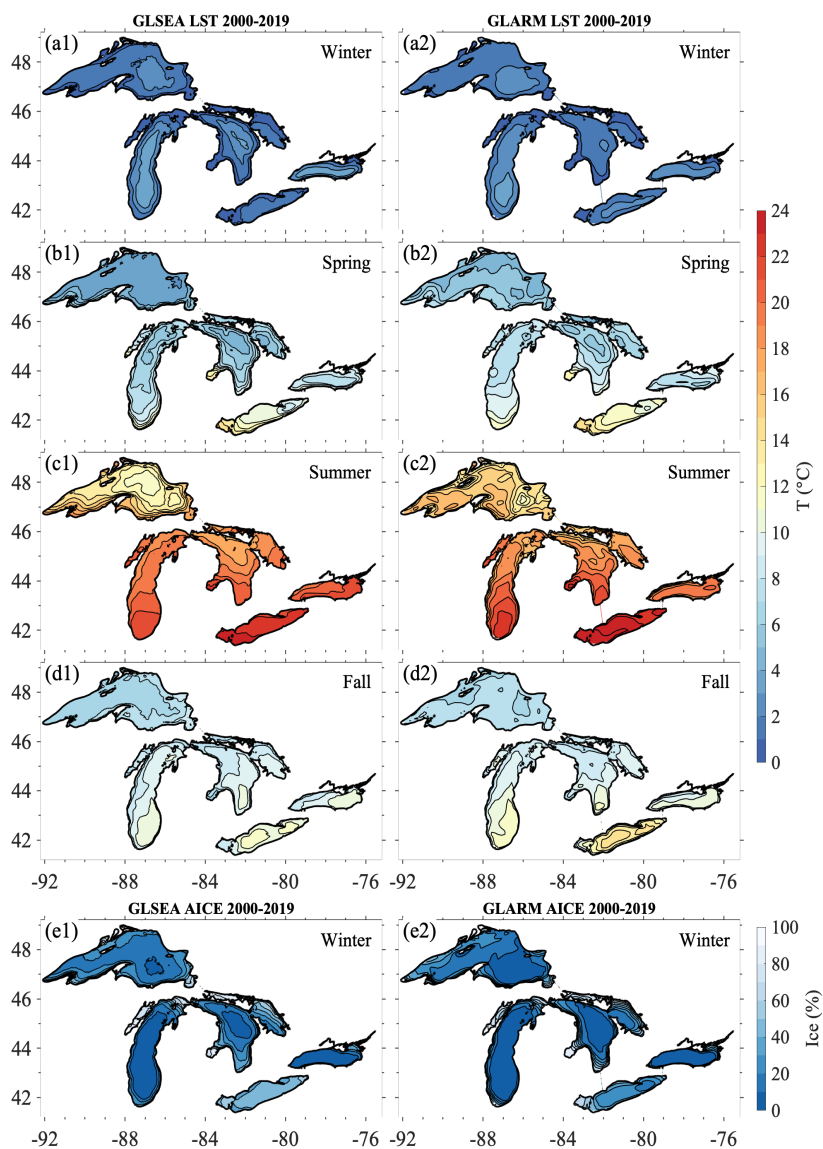


Figure 4: The LST seasonal climatologies (2000-2019) during (a1,a2) spring [April-June (AMJ)], (b1,b2) summer [July-September (JAS)], (c1,c2) fall [October-December (OND)], (d1,d2) winter [January-March (JFM)], and the ice cover climatologies (e1, e2). The GLSEA LST and GLICD ice observations are shown on the left panels; the GLARM-EA6 simulations are shown on the right panels.

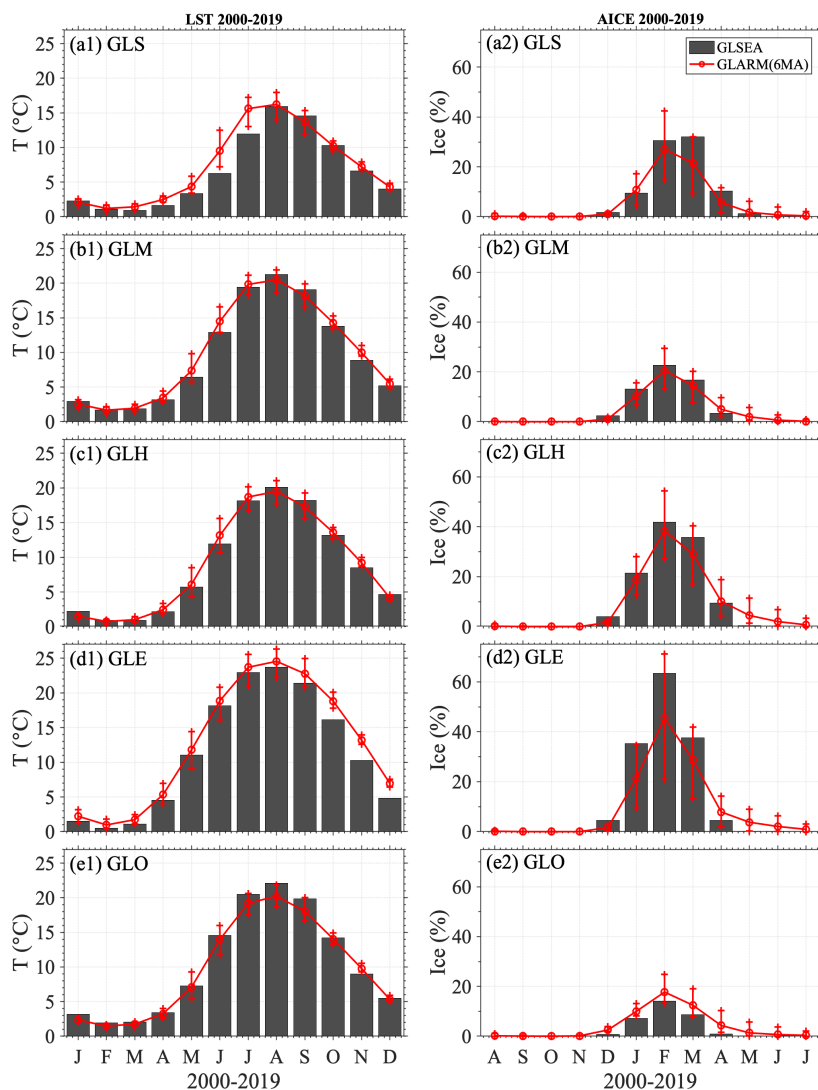


Figure 5: The monthly climatologies (2000-2019) of LST (left panels) and mean ice cover (right panels) in the five Great Lakes, respectively. The GLSEA LST and GLICD ice observations are shown in bar plots; the GLARM-EA6 simulations are shown in red lines with standard deviation of six GLARM configurations.

296 **3.2.2 Projected Climate Change**

297 **Surface Air Temperature**



298 Given the reliable performance of GLARM-EA6 in reproducing the present-day climate, we have
299 increased confidence that GLARM is capable of making meaningful scenario-based projections
300 of future climate. Here, we consider the RCP 4.5 and RCP 8.5 scenarios for the mid-century
301 (2030-2049) and late-century (2080-2099) relative to the early twenty-first century (2000-2019).
302 In the mid-century, the projected warming over the Great Lakes basin from two RCP scenarios
303 is relatively similar, which is consistent with the IPCC (2013, 2021) report. The annual surface
304 air temperature increases on average by 1.3°C in RCP 4.5 with a range of 0.8 to 1.9°C in six
305 individual projections, and 1.7°C in RCP 8.5 with a range of 1.3 to 2.2°C by the mid-century (Fig.
306 6-a,c). The late century projected warming is much more substantial with 2.3°C warming in RCP
307 4.5 (1.8 to 2.7°C) and 4.4°C in RCP 8.5 (4.0 to 4.9°C) (Fig. 6-b,d). Spatially, all projections
308 show a relatively higher increase by 0.1-0.5°C in the surface air temperature over land than over
309 lake depending on the scenario and time frame considered, revealing the cooling effect of the
310 lake. Such overlake and over-land temperature differences are most noticeable (4.0 vs. 4.5 °C)
311 by the end of the century in the RCP8.5 scenario. In the mid-century, larger uncertainty in the
312 projected surface air temperature, indicated by the standard deviation of the six-member ensemble
313 projections, appeared in the northern region. In the late-century projections, the lowest (highest)
314 uncertainties are found in the eastern part of the Great Lakes in RCP8.5 (RCP4.5) (Fig. 7).

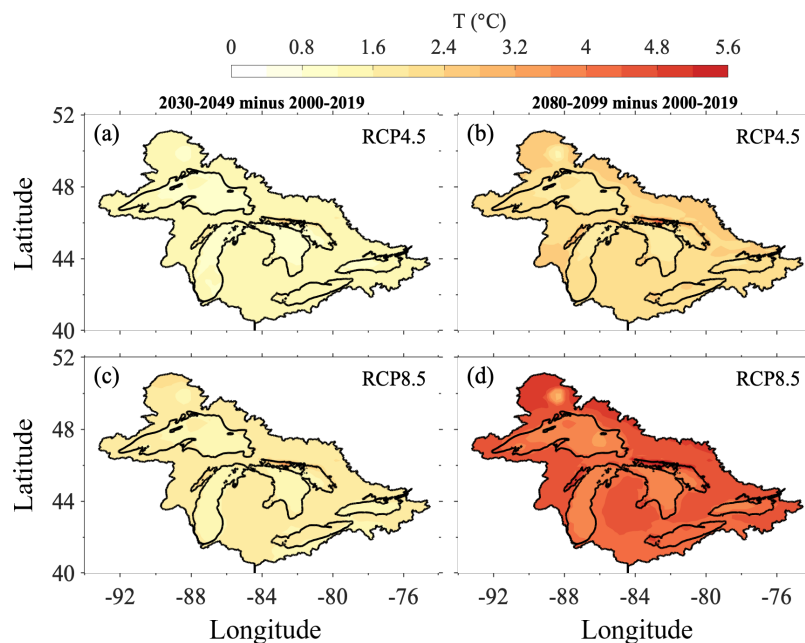


Figure 6: The changes in surface air temperature over the Great Lakes basin in the mid-century (2030-2049) and late-century (2080-2099) in RCP 4.5 and RCP 8.5 scenarios, predicted by GLARM-EA6.

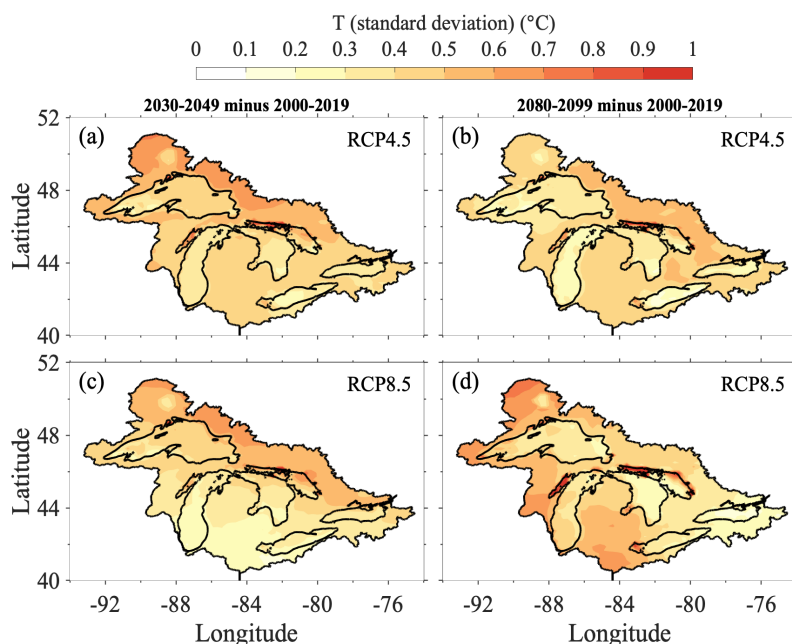


Figure 7: The uncertainties in GLARM-EA6 projected surface air temperature over the Great Lakes basin in the mid-century (2030-2049) and late-century (2080-2099) in RCP 4.5 and RCP 8.5 scenarios, indicated by the standard deviation of the six-member ensemble projections.

315 When considering monthly changes for each scenario and period averaged over the Great Lakes
316 basin, increases in air temperature are predicted to be similar from April to October in each
317 case (Fig. 8 and Table 3). More significant warming is projected during wintertime, which
318 is particularly noticeable in the mid-century. A larger increase in temperature is projected for
319 November and December for RCP 4.5 and December through March for RCP 8.5. By the end
320 of the century, the temperature increases showed less seasonal variability. As summarized in the
321 box-whisker plots of the six individual GLARM projections, the largest uncertainties across the
322 six models in the projected warming are during the cold seasons (October through April) with
323 variations of 2 to 3°C relative to the GLARM-EA6 ensemble mean, except for the late century in
324 RCP 8.5 scenario when the largest uncertainties occur from July through October.

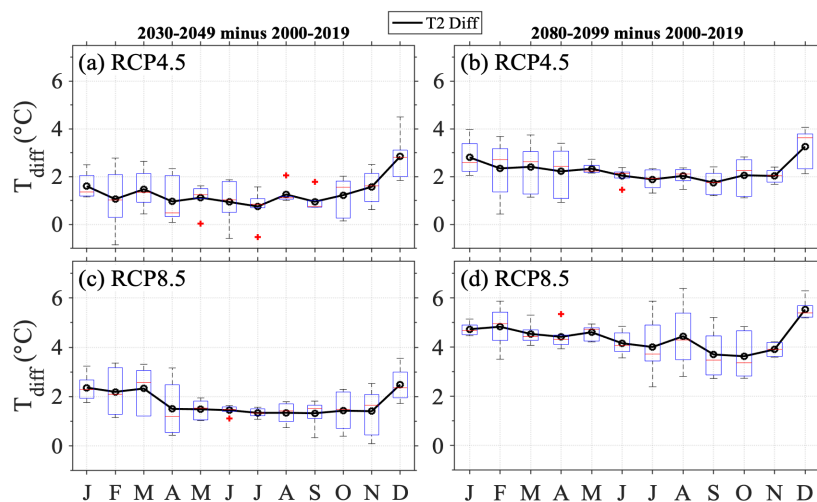


Figure 8: The average changes (black lines) in monthly surface air temperature over the Great Lakes basin in the mid-century (2030-2049) and late-century (2080-2099) in RCP 4.5 and RCP 8.5 scenarios, predicted by GLARM-EA6, uncertainties are indicated by the box-whisker plots based on from six individual GLARM projections.

325 **Precipitation**

326 The enhanced warming as a result of the increased atmospheric GHGs, results in increased precipitation
327 almost uniformly over the Great Lakes basin (Fig. 9 and Table 4). The projected mid-century
328 increase is greater for RCP 4.5 (6%) than for RCP 8.5 (4%) despite the relatively similar atmospheric
329 GHG concentrations over the period, confirming the lower degree of predictability of precipitation.
330 However, by the end of the century, when the differences in GHG forcing are substantial, the
331 precipitation increases are considerably greater for RCP 8.5 (18%) compared to RCP 4.5 (9%).
332 The larger mid-21st century increase under RCP 4.5 and the substantial increase under RCP 8.5
333 during the latter half of the century align with the results presented in Wuebbles et al. (2019).

334 The spatial variation of the precipitation increase by the late 21st century is more pronounced
335 under RCP 8.5 than RCP 4.5 (Fig. 9-b,d). Southern and western parts of the basin are projected
336 to experience the biggest precipitation increases, up to 28% in RCP 8.5 and 15% in RCP 4.5. The
337 uncertainties from GLARM precipitation projections show no clear spatial pattern, except for RCP
338 8.5 in which larger uncertainties are exhibited in the southwest region (Fig. 10). The standard
339 deviation of total precipitation of the six-member ensemble predictions increases from near 0.3
340 mm/day at the northern parts of the basin to near 1 mm/day at the southern parts of the basin.



Table 3: The GLARM-EA6 projected changes in monthly, seasonal, and annual surface air temperature over land, lake, and the Great Lakes basin in the mid-century and late-century in RCP 4.5 and RCP 8.5 scenarios, relative to the present-day climate (2000-2019).

	RCP4.5			RCP4.5			RCP8.5			RCP8.5		
	2030-2049			2080-2099			2030-2049			2080-2099		
	ΔT_2 (°C)			ΔT_2 (°C)			ΔT_2 (°C)			ΔT_2 (°C)		
	Basin	Lake	Land	Basin	Lake	Land	Basin	Lake	Land	Basin	Lake	Land
Jan	1.48	1.22	1.6	2.59	2.1	2.81	2.18	1.79	2.36	4.36	3.59	4.71
Feb	0.99	0.89	1.04	2.19	1.9	2.33	2.05	1.73	2.2	4.51	3.83	4.82
Mar	1.39	1.26	1.46	2.28	2.03	2.4	2.2	1.96	2.31	4.29	3.71	4.56
Apr	0.92	1.03	0.87	2.13	2.09	2.15	1.44	1.51	1.4	4.22	4	4.33
May	1.09	1.28	1.01	2.27	2.45	2.19	1.45	1.74	1.32	4.48	4.81	4.33
Jun	0.96	1.24	0.83	2.08	2.4	1.93	1.47	1.82	1.32	4.22	4.72	3.99
Jul	0.78	0.88	0.73	1.94	1.98	1.92	1.38	1.51	1.32	4.11	4.1	4.11
Aug	1.27	1.18	1.31	2.05	1.94	2.1	1.36	1.28	1.39	4.48	4.15	4.63
Sep	1.09	1.03	1.12	2	1.87	2.06	1.52	1.33	1.6	4.23	3.83	4.41
Oct	1.35	1.18	1.43	2.27	2.05	2.37	1.57	1.37	1.67	3.99	3.62	4.16
Nov	1.7	1.43	1.82	2.19	1.9	2.32	1.52	1.29	1.62	4.2	3.72	4.42
Dec	2.67	2.13	2.92	3.06	2.43	3.35	2.34	1.89	2.54	5.18	4.25	5.61
JFM	1.29	1.12	1.36	2.35	2.01	2.51	2.14	1.83	2.29	4.39	3.71	4.7
AMJ	0.99	1.18	0.9	2.16	2.31	2.09	1.45	1.69	1.35	4.31	4.51	4.22
JAS	1.05	1.03	1.05	2	1.93	2.03	1.42	1.37	1.44	4.27	4.03	4.38
OND	1.91	1.58	2.06	2.5	2.13	2.68	1.81	1.52	1.94	4.46	3.86	4.73
Annual	1.31	1.23	1.34	2.25	2.1	2.33	1.71	1.6	1.75	4.36	4.03	4.51

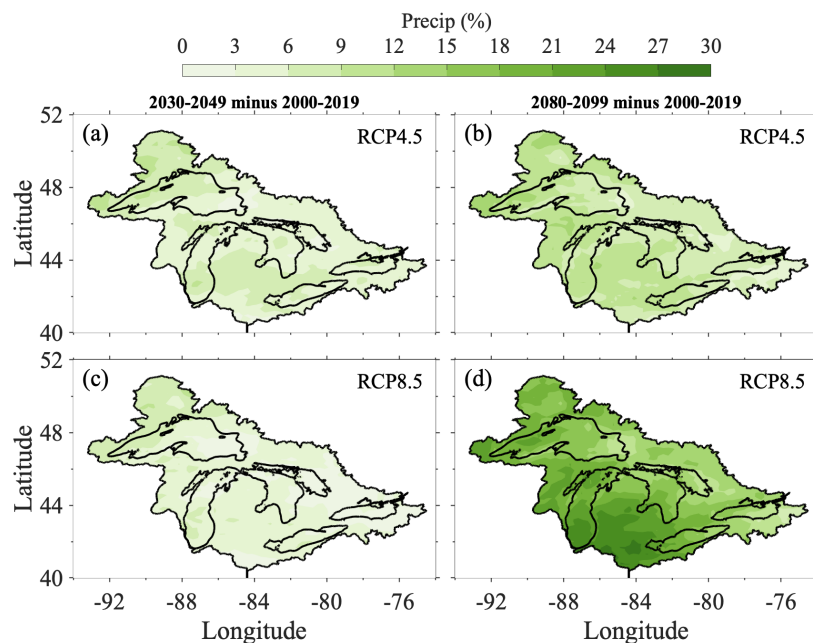


Figure 9: The project GLARM-EA6 changes in total precipitation over the Great Lakes basin in the mid-21st century (2030-2049) and late-21st century (2080-2099) in RCP 4.5 and RCP 8.5 scenarios.

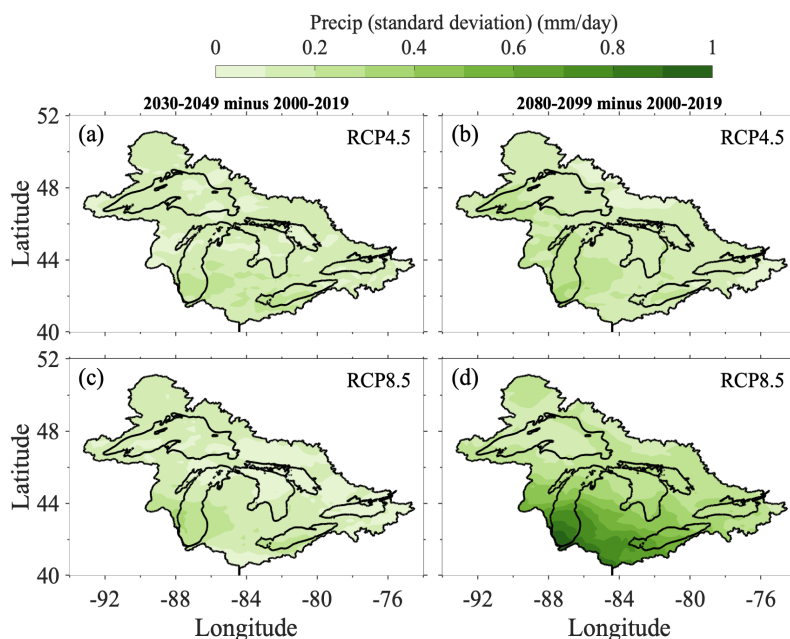


Figure 10: The uncertainties in GLARM-EA6 projected precipitation over the Great Lakes basin in the mid-century (2030–2049) and late century (2080–2099) in RCP 4.5 and RCP 8.5 scenarios, indicated by the standard deviation of the six-member ensemble projections.

341 Seasonally, while the GLARM-EA6 average shows basin-wide precipitation increases in nearly
342 all months, the predictions differ considerably between the individual six ensemble members (Fig.
343 11). The strongest and most robust signal is projected in spring, particularly in April and May,
344 which is found in all cases and is consistent with several previous studies (Byun and Hamlet 2018;
345 Notaro et al. 2015; Zhang et al. 2020). Not consistent with the aforementioned studies is that
346 GLARM-EA6 projects the enhanced spring precipitation persists into the summer at the end of the
347 century.

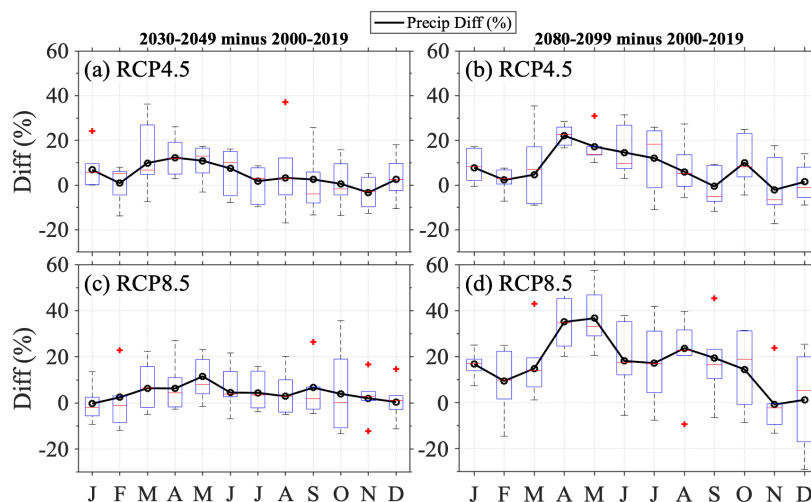


Figure 11: The average changes (black lines) in monthly surface precipitation over the Great Lakes basin in the mid-century (2030-2049) and late-century (2080-2099) in RCP 4.5 and RCP 8.5 scenarios, predicted by GLARM-EA6, uncertainties are indicated by the box-whisker plots based on from six individual GLARM projections.

348 Lake Surface Temperature

349 LST variability in each of the Great Lakes is significantly influenced by depth and geographic
350 characteristics. The shallower lakes like Lake Erie exhibit larger seasonal LST variability than the
351 deeper lakes like Lake Superior (e.g., summer LSTs are $>25^{\circ}\text{C}$ in Lake Erie and $<18^{\circ}\text{C}$ in Lake
352 Superior). Similar to the surface air temperature warming in the basin, the LSTs in the five lakes are
353 projected to increase in time as the atmospheric GHGs accumulate (Table 5). The most significant
354 LST increase occurs in Lake Superior under both RCP scenarios, followed by Lakes Michigan,
355 Huron, Ontario, and Erie. Here we highlight the strong seasonal variability in lake warming as
356 opposed to the seasonal pattern of surface air temperature increase (Fig. 12). In contrast to surface
357 air temperature which shows little seasonal variability in its change, the LST increases in the lakes
358 show substantial seasonal variability with the greatest changes projected in May and June in four
359 of the five lakes. For example, the Lake Superior LSTs increase by 6.1°C and 3.2°C at the end of
360 the century in RCP 8.5 and RCP 4.5, respectively, which are significantly larger than the annual
361 mean respective increases of 4.1°C and 2.0°C (Fig. 12). As the summer progresses, the amplified
362 warming begins to decline until the winter where it reaches its minimum increase of approximately
363 3°C in RCP 8.5 and 2°C in RCP 4.5 in the late-century. This is likely a result of some of the energy
364 being used for ice melting and heat being transferred to the deepwater under unstratified conditions.
365 Such patterns are projected across the lakes under all scenarios and for all periods, except for Lake



Table 4: The GLARM-EA6 projected changes in monthly, seasonal, and annual precipitation over land, lake, and the Great Lakes basin in the mid-century and late-century in RCP 4.5 and RCP 8.5 scenarios, relative to the present-day climate (2000-2019).

	RCP4.5			RCP4.5			RCP8.5			RCP8.5		
	2030-2049			2080-2099			2030-2049			2080-2099		
	ΔP (%)			ΔP (%)			ΔP (%)			ΔP (%)		
	Basin	Lake	Land	Basin	Lake	Land	Basin	Lake	Land	Basin	Lake	Land
Jan	4.86	2.02	6.31	5.57	1.52	7.64	-0.2	-3.29	1.38	11.98	4.34	15.87
Feb	0.63	-0.82	1.33	1.68	-0.11	2.55	1.83	-0.06	2.74	7	2.7	9.07
Mar	9.24	8.92	9.39	4.38	4.87	4.16	6	5.66	6.16	13.93	13.19	14.25
Apr	12.22	11.96	12.33	22.03	22.05	22.03	6.28	5.18	6.77	34.95	35.41	34.75
May	10.88	12.86	10.03	17.22	19.29	16.34	11.52	12.76	11	36.63	40.52	34.97
Jun	7.63	8.51	7.25	14.98	16.26	14.42	4.64	4.94	4.51	18.63	19.92	18.08
Jul	1.85	2.21	1.7	12.6	14.35	11.83	4.63	5.83	4.1	18.06	21.95	16.35
Aug	3.23	4.92	2.47	5.95	8.11	5	2.92	4.66	2.15	23.77	27.9	21.94
Sep	2.96	3.34	2.79	-0.72	0.78	-1.41	7.84	8.31	7.62	22.88	22.21	23.19
Oct	0.52	0.74	0.42	9.29	9.16	9.35	3.67	3.53	3.73	13.39	14.07	13.09
Nov	6.38	4.61	7.21	4.06	2.6	4.75	-3.87	-4.53	-3.56	1.5	-0.94	2.64
Dec	6.63	3.71	8.06	3.88	0.5	5.55	1.17	-0.87	2.18	3.29	-2.02	5.91
JFM	4.91	3.37	5.68	3.88	2.09	4.78	2.54	0.77	3.42	10.97	6.75	13.07
AMJ	10.24	11.11	9.87	18.08	19.2	17.59	7.48	7.63	7.42	30.07	31.95	29.26
JAS	2.68	3.49	2.32	5.94	7.75	5.14	5.13	6.27	4.62	21.57	24.02	20.49
OND	4.51	3.02	5.23	5.75	4.09	6.55	0.32	-0.62	0.78	6.06	3.7	7.21
Annual	5.59	5.25	5.78	8.41	8.28	8.52	3.87	3.51	4.06	17.17	16.6	17.51



366 Erie which is projected to have the largest increase in summer. Spatially, the offshore waters where
 367 depths are greatest are projected to experience the most significant warming across the lakes (Fig.
 368 13).

Table 5: The GLARM-EA6 projected changes in annual LST in the five Great Lakes basins in the mid-century (2030-2049) and late century (2080-2099) in RCP 4.5 and RCP 8.5 scenarios, relative to the present-day climate (2000-2019).

	RCP4.5			RCP4.5			RCP8.5			RCP8.5		
	2030-2049			2080-2099			2030-2049			2080-2099		
	Δ LST(°C)			Δ LST(°C)			Δ LST(°C)			Δ LST(°C)		
	Min	Mean	Max	Min	Mean	Max	Min	Mean	Max	Min	Mean	Max
GLS	0.87	1.16	1.52	1.77	1.97	2.38	1.18	1.56	2.11	3.96	4.11	4.53
GLM	0.79	1.12	1.51	1.66	1.86	2.21	1.21	1.51	1.95	3.71	3.98	4.57
GLH	0.75	0.99	1.3	1.55	1.77	2.04	1.02	1.33	1.72	3.48	3.66	4.15
GLE	0.51	0.81	1.07	1.08	1.37	1.52	0.56	0.95	1.16	2.4	2.73	3.02
GLO	0.89	1.15	1.5	1.8	2.03	2.27	1.18	1.45	1.93	3.96	4.15	4.44

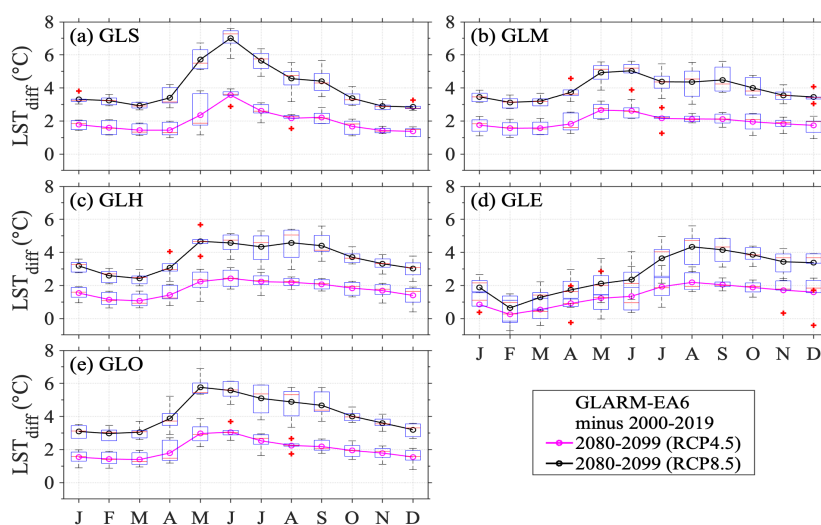


Figure 12: The average changes (black and purple lines) in LSTs over the five Great Lakes in the late-century (2080-2099) in RCP 4.5 and RCP 8.5 scenarios, predicted by GLARM-EA6, uncertainties are indicated by the box-whisker plots based on the six-member ensemble projections.

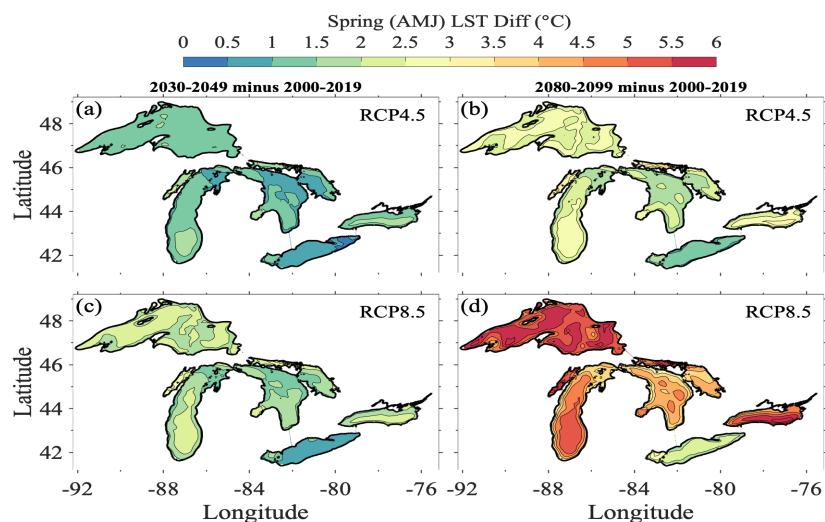


Figure 13: The changes in spring (AMJ) LSTs over the Great Lakes basin in the mid-century (2030-2049) and late-century (2080-2099) in RCP 4.5 and RCP 8.5 scenarios, predicted by GLARM-EA6.

369 Lake Ice

370 In the winter, the warming signals are reflected in an overall reduction in ice coverage and duration
371 (Fig. 14) in all scenarios and periods. Here we present the projected lake conditions in the
372 late-century as an example (Fig. 14). The ice cover projections show the least uncertainty in RCP
373 8.5 scenario in the late-century, in response to the strongest warming. In the RCP 8.5 scenario,
374 mean ice coverage in February is projected to reduce to between 3% and 6% across the lakes. This
375 indicates that ice cover percentage in the five lakes will become more uniform compared to the
376 present-day conditions (Fig. 5). The ice duration (defined with a threshold of 10% ice coverage at
377 a given model grid) is projected to decrease correspondingly (Fig. 15). By the mid-21st century,
378 the ice duration is projected to decrease by 5 to 25 days depending on the scenario and location;
379 and by the late century up to 50 days in the coastal regions where higher ice covers are typical in
380 the present-day climate.

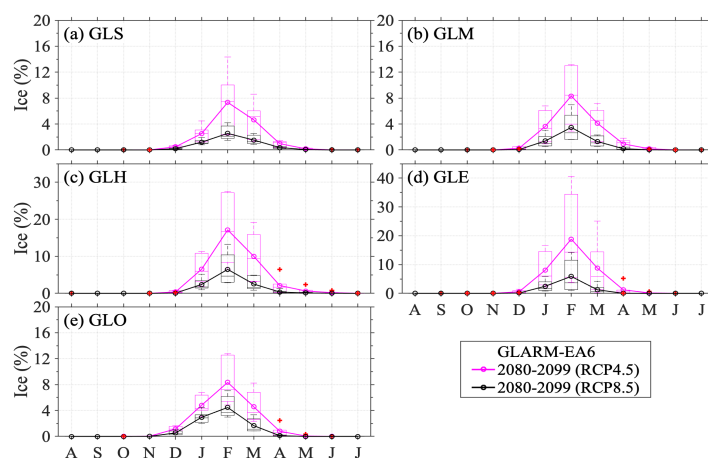


Figure 14: The projected monthly mean ice covers in the five Great Lakes in the late century (2080-2099) in RCP 4.5 and RCP 8.5 scenarios, predicted by GLARM-EA6, uncertainties are indicated by the box-whisker plots based on the six-member ensemble projections.

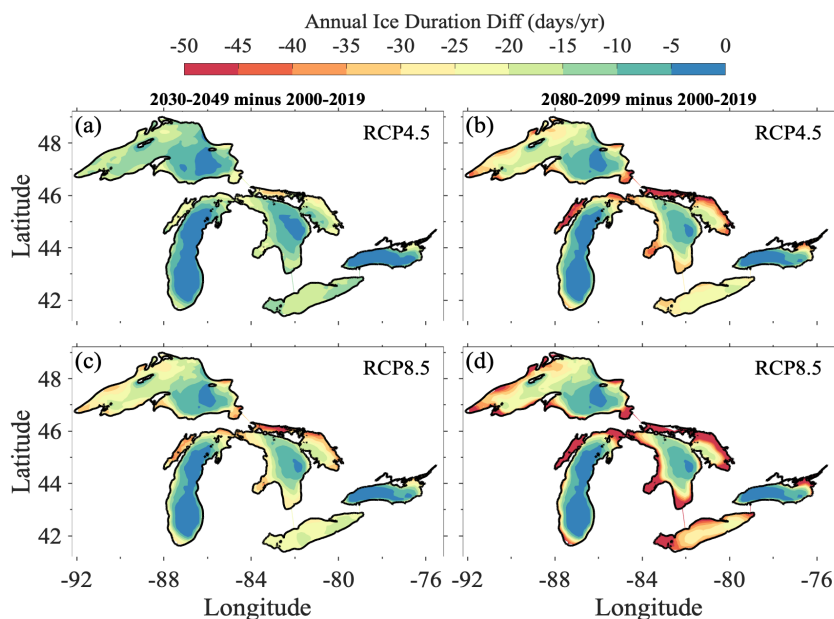


Figure 15: The reduction in ice duration (days) in the Great Lakes in the mid-century (2030-2049) and late-century (2080-2099) in RCP 4.5 and RCP 8.5 scenarios, predicted by GLARM-EA6.



381 **4 Discussion and Conclusions**

382 **4.1 Model Advancement**

383 The Great Lakes are a key element in regional climate of the basin and play an important role
384 in influencing local weather patterns and climate processes. Climate processes are changing,
385 accompanied by changes in the Great Lakes. Many of these complex changes are regulated by
386 interactions among the atmosphere, lake, ice, and surrounding land areas that can also have an
387 important influence in regulating regional climate. The lack of fully integrated regional models
388 that resolve 3-D lake dynamics may result in inaccurate projections of climate change for the
389 basin and associated adaptation and mitigation measures. To the best of our knowledge, this study
390 presents the first climate change projections including both the Great Lakes basin and the changes
391 in the five Great Lakes that has employed a two-way coupled regional climate model with a 3-D
392 lake model (i.e. GLARM).

393 Using the three carefully selected CMIP5 AOGCMS and two domains (large continental and small
394 regional), we show that the GLARM six-member ensemble average (GLARM-EA6) substantially
395 reduces the surface air temperature and precipitation biases of the driving AOGCM ensemble
396 average. The improvements are not only displayed from the atmospheric perspective but also
397 include lake surface temperature and ice coverage and duration.

398 **4.2 Summary of Climate Projections**

399 The GLARM climate change projections are performed for the mid-century (2030-2049) and
400 late-century (2080-2099) for the RCP 8.5 "business as usual" scenario and the RCP 4.5 moderate
401 mitigation scenario. The surface air temperature over the Great Lakes Basin is projected to increase
402 in all months regardless of the scenario, period of consideration and ensemble member. Under RCP
403 8.5, the Great Lakes basin is projected to warm by 1.3-2.2°C by the mid-21st century and 4.0-4.9°C
404 by the end of the century relative to the early-century (2000-2019). Moderate mitigation (RCP 4.5)
405 reduces the mid-century warming to 0.8-1.9°C and late-century warming to 1.8-2.7°C. The largest
406 amount of warming is projected during the winter, consistent with the predictions from Byun and
407 Hamlet (2018) and Zhang et al. (2020). Since previous studies consider different time periods and
408 GHG emissions scenarios for their projections, a comparison of precise magnitude of changes
409 is not possible; nevertheless qualitative comparisons can be made. The GLARM simulations
410 presented here project surface air temperature increases slightly smaller than those of previous
411 studies (e.g., Notaro et al. 2015; Zhang et al. 2020). For example, by 2080-2099 under RCP 8.5,
412 Notaro et al. (2015) project annual overland air temperature to increase by up to 5.9°C relative to
413 1980-1999, while GLARM predicts an increase of 4.5°C relative to 2000-2019. When considering
414 that the CRU data show a 0.5°C difference between the baseline periods of the two studies, the
415 GLARM RCP 8.5 ensemble projects a reduction by about 0.9°C compared to Notaro et al. (2015).



416 As for the spatial variation of the predicted increase, GLARM's relatively larger increase in the
417 northern part of the basin (particularly under RCP 4.5 by the end of the 21st century) agrees with
418 Xiao et al. (2018).

419 Annual precipitation in GLARM is projected to increase for the entire basin with the largest
420 relative increases in spring and early summer when current precipitation is highest and little
421 increase in winter when it is lowest. There is some consensus among previous studies at the
422 annual timescale, However, these studies project decreases in summer and increases in winter and
423 spring (e.g., Byun and Hamlet 2018; Notaro et al. 2015; Zhang et al. 2020). In addition, the
424 smaller Great Lakes domain configuration projects a wider range of precipitation suggesting that
425 the dynamics over the Great Lakes region are more constrained by the lateral boundary conditions
426 and inherit precipitation patterns from the driving AOGCMs. This is particularly evident for
427 the MPI-ECM-MR downscaling cases where the projected increases are relatively large with the
428 smaller GLARM domain and muted changes with the larger domain. This reinforces the use of
429 two different modeling domains The large North America domain to account for both dynamic
430 consistency of climate processes resolved in the GLARM and allow the regional scale feature to
431 fully develop; Meanwhile, the small domain GLARM, similar to other RCM configuration for the
432 Great Lakes climate study to represent the uncertainty inherited from different GCMs and enhance
433 computational efficiency.

434 LST also increases across the five lakes in all of the simulations, but with a stronger seasonal
435 signature compared to surface air temperature which was relatively constant in all months. The
436 strongest warming was projected in spring followed by strong summer warming suggesting earlier
437 and more intense stratification in the future. In contrast, a relatively small increase in fall and winter
438 LST is projected with a minimal increase with heat transfer to the deepwater due to strong mixing
439 and energy required for ice melting. Correspondingly, GLARM ensemble projects decreased ice
440 cover and duration. Of particular note, the highest monthly mean ice cover is projected to be only
441 3 to 6% across the lakes by the end of the 21st century in RCP 8.5; and ice duration will decrease
442 by up to 30- 50 days in the coastal regions. The few climate change studies that dynamically
443 downscale Great lake temperatures and ice cover used 1-D lake models embedded in the RCMs
444 (Notaro et al. 2015; Xiao et al. 2018). The GLARM simulations are consistent with these previous
445 studies, however, the magnitude of the increase is considerably less than Xiao et al. (2018) who
446 project increases of 3.5 to 4.0 °C for 2070-2100 relative to 1975-2005 under RCP 4.5 and Notaro
447 et al. (2015) who project increases of up to 8°C by 2080-2099 relative to 1980-1999 under RCP 8.5.
448 Counterintuitively, both of these studies project larger ice coverage than the GLARM's simulation.
449 It should be noted that their ice coverage simulations were heavily limited by their 1D lake-ice
450 model; both studies explicitly noted that the absence of 3D model produced substantial summer
451 warm biases and cold biases in winter (Notaro et al. 2015) with earlier ice onset and excessive
452 mid-winter ice (Xiao et al. 2018). Hence, the 3D representation of lake and ice processes within
453 GLARM could feedback to dampen changes in lake warming and ice coverage and duration.



454 Collectively, the projected changes in the atmosphere and the lakes are expected to modify weather
455 and climate extremes and associated coastal hazards, including extended local heat stresses and
456 marine (lake) heatwaves, heavy precipitation, rising lake levels, and coastal flooding (Huang et al.
457 2021a,b; Notaro et al. 2021; Wuebbles et al. 2019; Zhang et al. 2019). With unabated GHG gas
458 emissions, all lakes will experience less ice coverage extent and duration and even ice-free winters.
459 This will significantly alter the overlake heat and moisture fluxes during the cold season, which
460 could lead to intensified winter storms. For example, the increased winter moisture supply from
461 the lakes along with events of cold air mass (e.g. polar vortex) can create ideal conditions stronger
462 lake effect snowfall events (Basile et al. 2017; d’Orgeville et al. 2014). As such, we advocate
463 that a regional earth system modeling system with integration of observing networks becomes
464 vitally essential to guide decision-makers in response to climate change and climate-driven coastal
465 hazards.

466 **Author Contributions:** Conceptualization, P.X.; methodology, P.X., X. Y, C. H., J.S.P.; software,
467 P.X., X.Y, C. H.; validation, C.H., X.Y.; visualization, C.H., formal analysis, P.X., J.S.P., P.Y.C.,
468 X.Y., M.B.K.; resources, P.X.; writing—original draft preparation, P.X., M.B.K.; J.S.P.; writing—review
469 and editing, P.X., J.S.P., P.Y.C.; supervision, P.X.; project administration, P.X.; funding acquisition,
470 P.X. All authors have read and agreed to the published version of the manuscript.

471 **Funding:** This research was partly supported by the National Aeronautics and Space Administration,
472 Grant 80NSSC17K0287. Hydrodynamic modeling was also supported, in part, by COMPASS-GLM,
473 a multi-institutional project supported by the U.S. Department of Energy, Office of Science, Office
474 of Biological and Environmental Research, Earth and Environmental Systems Modeling program.

475 **Data Availability:** The Great Lakes Surface Environmental Analysis (GLSEA) is available from
476 <https://coastwatch.glerl.noaa.gov/glsea/glsea.html>. The Great Lakes Ice Cover Database
477 (GLICD) is available from <https://www.glerl.noaa.gov/data/ice/#historical>. The RegCM4
478 code is available through <https://www.ictp.it/research/esp/models/regcm4.aspx>. The
479 CRU data is available from <https://crudata.uea.ac.uk/cru/data/hrg/#current> The FVCOM
480 code is available through <http://fvcom.smast.umassd.edu/fvcom/>. Further inquiries can be
481 directed to the corresponding author.

482 **Acknowledgments:** This is the contribution XX of the Great Lakes Research Center at Michigan
483 Technological University. The Michigan Tech high-performance computing cluster, *Superior*, was
484 used in obtaining the hydrodynamic modeling results presented in this publication.

485 **Conflicts of Interest:** The authors declare no conflict of interest.



486 References

- 487 Anderson, E. J., Fujisaki-Manome, A., Kessler, J., Lang, G. A., Chu, P. Y., Kelley, J. G., Chen, Y.,
488 and Wang, J. (2018). “Ice forecasting in the next-generation Great Lakes operational forecast
489 system (GLOFS)”. *Journal of Marine Science and Engineering* 6.4, p. 123.
- 490 Austin, J. and Colman, S. (2008). “A century of temperature variability in Lake Superior”. *Limnology
491 and Oceanography* 53.6, pp. 2724–2730.
- 492 Austin, J. A. and Colman, S. M. (2007). “Lake Superior summer water temperatures are increasing
493 more rapidly than regional air temperatures: A positive ice-albedo feedback”. *Geophysical
494 Research Letters* 34.6.
- 495 Basile, S. J., Rauscher, S. A., and Steiner, A. L. (2017). “Projected precipitation changes within the
496 Great Lakes and Western Lake Erie Basin: a multi-model analysis of intensity and seasonality”.
497 *International Journal of Climatology* 37.14, pp. 4864–4879.
- 498 Bennington, V., Notaro, M., and Holman, K. D. (2014). “Improving climate sensitivity of deep
499 lakes within a regional climate model and its impact on simulated climate”. *Journal of Climate*
500 27.8, pp. 2886–2911.
- 501 Briley, L. J., Rood, R. B., and Notaro, M. (2021). “Large lakes in climate models: A Great Lakes
502 case study on the usability of CMIP5”. *Journal of Great Lakes Research* 47.2, pp. 405–418.
- 503 Byun, K., Chiu, C.-M., and Hamlet, A. F. (2019). “Effects of 21st century climate change on
504 seasonal flow regimes and hydrologic extremes over the Midwest and Great Lakes region of
505 the US”. *Science of the Total Environment* 650, pp. 1261–1277.
- 506 Byun, K. and Hamlet, A. F. (2018). “Projected changes in future climate over the Midwest and
507 Great Lakes region using downscaled CMIP5 ensembles”. *International Journal of Climatology*
508 38, e531–e553.
- 509 Chen, C., Beardsley, R., Cowles, G., Qi, J., Lai, Z., Gao, G., Stuebe, D., Xu, Q., Xue, P., Ge, J., et al.
510 (2012). *An unstructured-grid, finite-volume community ocean model: FVCOM user manual*.
511 Sea Grant College Program, Massachusetts Institute of Technology Cambridge
- 512 Cherkauer, K. A. and Sinha, T. (2010). “Hydrologic impacts of projected future climate change in
513 the Lake Michigan region”. *Journal of Great Lakes Research* 36, pp. 33–50.
- 514 Collingsworth, P. D., Bunnell, D. B., Murray, M. W., Kao, Y.-C., Feiner, Z. S., Claramunt, R. M.,
515 Lofgren, B. M., Höök, T. O., and Ludsins, S. A. (2017). “Climate change as a long-term stressor
516 for the fisheries of the Laurentian Great Lakes of North America”. *Reviews in Fish Biology
517 and Fisheries* 27.2, pp. 363–391.
- 518 d’Orgeville, M., Peltier, W. R., Erler, A. R., and Gula, J. (2014). “Climate change impacts on Great
519 Lakes Basin precipitation extremes”. *Journal of Geophysical Research: Atmospheres* 119.18,
520 pp. 10–799.



- 521 Dalolu, I., Cho, K. H., and Scavia, D. (2012). “Evaluating causes of trends in long-term dissolved
522 reactive phosphorus loads to Lake Erie”. *Environmental Science & Technology* 46.19, pp. 10660–10666.
- 523 Delaney, F. and Milner, G. (2019). “The State of Climate Modeling in the Great Lakes Basin-A
524 Synthesis in Support of a Workshop held on June 27, 2019 in Ann Arbor, MI.”
- 525 Dobiesz, N. E. and Lester, N. P. (2009). “Changes in mid-summer water temperature and clarity
526 across the Great Lakes between 1968 and 2002”. *Journal of Great Lakes Research* 35.3,
527 pp. 371–384.
- 528 EPA, U. (2014). *State of the Great Lakes 2011*. Tech. rep. EPA 950-R-13-002.
- 529 Fujisaki, A., Wang, J., Bai, X., Leshkevich, G., and Lofgren, B. (2013). “Model-simulated interannual
530 variability of Lake Erie ice cover, circulation, and thermal structure in response to atmospheric
531 forcing, 2003–2012”. *Journal of Geophysical Research: Oceans* 118.9, pp. 4286–4304.
- 532 Fujisaki, A., Wang, J., Hu, H., Schwab, D. J., Hawley, N., and Rao, Y. R. (2012). “A modeling
533 study of ice–water processes for Lake Erie applying coupled ice-circulation models”. *Journal
534 of Great Lakes Research* 38.4, pp. 585–599.
- 535 Giorgi, F., Coppola, E., Solmon, F., Mariotti, L., Sylla, M., Bi, X., Elguindi, N., Diro, G., Nair, V.,
536 Giuliani, G., et al. (2012). “RegCM4: model description and preliminary tests over multiple
537 CORDEX domains”. *Climate Research* 52, pp. 7–29.
- 538 Giorgi, F. and Mearns, L. O. (2002). “Calculation of average, uncertainty range, and reliability of
539 regional climate changes from AOGCM simulations via the reliability ensemble averaging (REA)
540 method”. *Journal of climate* 15.10, pp. 1141–1158.
- 541 Gula, J. and Peltier, W. R. (2012). “Dynamical downscaling over the Great Lakes basin of North
542 America using the WRF regional climate model: The impact of the Great Lakes system on
543 regional greenhouse warming”. *Journal of Climate* 25.21, pp. 7723–7742.
- 544 Harris, I., Jones, P. D., Osborn, T. J., and Lister, D. H. (2014). “Updated high-resolution grids of
545 monthly climatic observations—the CRU TS3. 10 Dataset”. *International journal of climatology*
546 34.3, pp. 623–642.
- 547 Hayhoe, K., VanDorn, J., Croley II, T., Schlegel, N., and Wuebbles, D. (2010). “Regional climate
548 change projections for Chicago and the US Great Lakes”. *Journal of Great Lakes Research*
549 36, pp. 7–21.
- 550 Hostetler, S. W., Bates, G. T., and Giorgi, F. (1993). “Interactive coupling of a lake thermal
551 model with a regional climate model”. *Journal of Geophysical Research: Atmospheres* 98.D3,
552 pp. 5045–5057.
- 553 Huang, C., Anderson, E., Liu, Y., Ma, G., Mann, G., and Xue, P. (2021a). “Evaluating essential
554 processes and forecast requirements for meteotsunami-induced coastal flooding”. *Natural
555 Hazards*, pp. 1–26.



- 556 Huang, C., Kuczynski, A., Auer, M. T., ODonnell, D. M., and Xue, P. (2019). “Management
557 transition to the Great Lakes nearshore: Insights from hydrodynamic modeling”. *Journal of*
558 *Marine Science and Engineering* 7.5, p. 129.
- 559 Huang, C., Zhu, L., Ma, G., Meadows, G. A., and Xue, P. (2021b). “Wave Climate Associated
560 With Changing Water Level and Ice Cover in Lake Michigan”. *Frontiers in Marine Science*.
- 561 Ibrahim, H. D., Xue, P., and Eltahir, E. A. (2020). “Multiple salinity equilibria and resilience of
562 Persian/Arabian Gulf basin salinity to brine discharge”. *Frontiers in Marine Science* 7, p. 573.
- 563 IPCC (2013). “IPCC 2013: Climate change 2013: the physical science basis: Working Group I
564 contribution to the Fifth assessment report of the Intergovernmental Panel on Climate Change”.
- 565 — (2021). “IPCC, 2021: Climate Change 2021: The Physical Science Basis. Contribution of
566 Working Group I to the Sixth Assessment Report of the Intergovernmental Panel on Climate
567 Change.”
- 568 Jones, M. L., Shuter, B. J., Zhao, Y., and Stockwell, J. D. (2006). “Forecasting effects of climate
569 change on Great Lakes fisheries: models that link habitat supply to population dynamics can
570 help”. *Canadian Journal of Fisheries and Aquatic Sciences* 63.2, pp. 457–468.
- 571 Lynch, A. J., Myers, B. J., Chu, C., Eby, L. A., Falke, J. A., Kovach, R. P., Krabbenhoft, T. J.,
572 Kwak, T. J., Lyons, J., Paukert, C. P., et al. (2016). “Climate change effects on North American
573 inland fish populations and assemblages”. *Fisheries* 41.7, pp. 346–361.
- 574 MacKay, M. and Seglenieks, F. (2013). “On the simulation of Laurentian Great Lakes water levels
575 under projections of global climate change”. *Climatic Change* 117.1, pp. 55–67.
- 576 Mailhot, E., Music, B., Nadeau, D. F., Frigon, A., and Turcotte, R. (2019). “Assessment of the
577 Laurentian Great Lakes hydrological conditions in a changing climate”. *Climatic Change*
578 157.2, pp. 243–259.
- 579 McCormick, M. J. and Fahnenstiel, G. L. (1999). “Recent climatic trends in nearshore water
580 temperatures in the St. Lawrence Great Lakes”. *Limnology and Oceanography* 44.3, pp. 530–540.
- 581 Melillo, J. M., Richmond, T., Yohe, G., et al. (2014). “Climate change impacts in the United
582 States”. *Third national climate assessment* 52.
- 583 Music, B., Frigon, A., Lofgren, B., Turcotte, R., and Cyr, J.-F. (2015). “Present and future Laurentian
584 Great Lakes hydroclimatic conditions as simulated by regional climate models with an emphasis
585 on Lake Michigan-Huron”. *Climatic Change* 130.4, pp. 603–618.
- 586 Notaro, M., Bennington, V., and Vavrus, S. (2015). “Dynamically downscaled projections of lake-effect
587 snow in the Great Lakes basin”. *Journal of Climate* 28.4, pp. 1661–1684.
- 588 Notaro, M., Zhong, Y., Xue, P., Peters-Lidard, C., Cruz, C., Kemp, E., Kristovich, D., Kulie, M.,
589 Wang, J., Huang, C., et al. (2021). “Cold Season Performance of the NU-WRF Regional
590 Climate Model in the Great Lakes Region”. *Journal of Hydrometeorology* 22.9, pp. 2423–2454.



- 591 Pal, J. S., Giorgi, F., Bi, X., Elguindi, N., Solmon, F., Gao, X., Rauscher, S. A., Francisco, R.,
592 Zakey, A., Winter, J., et al. (2007). “Regional climate modeling for the developing world:
593 the ICTP RegCM3 and RegCNET”. *Bulletin of the American Meteorological Society* 88.9,
594 pp. 1395–1410.
- 595 Poesch, M. S., Chavarie, L., Chu, C., Pandit, S. N., and Tonn, W. (2016). “Climate change impacts
596 on freshwater fishes: a Canadian perspective”. *Fisheries* 41.7, pp. 385–391.
- 597 Pryor, S. C., Scavia, D., Downer, C., Gaden, M., Iverson, L., Nordstrom, R., Patz, J., and Robertson,
598 G. P. (2014). “Midwest. Climate change impacts in the United States: The third national
599 climate assessment”. In: *Melillo, JM; Richmond, TC; Yohe, GW, eds. National Climate Assessment*
600 *Report. Washington, DC: US Global Change Research Program: 418-440.*, pp. 418–440.
- 601 Rau, E., Vaccaro, L., Riseng, C., and Read, J. (2020). *The dynamic great lakes economy employment*
602 *trends from 2009 to 2018.*
- 603 Scavia, D., Allan, J. D., Arend, K. K., Bartell, S., Beletsky, D., Bosch, N. S., Brandt, S. B., Briland,
604 R. D., Dalolu, I., DePinto, J. V., et al. (2014). “Assessing and addressing the re-eutrophication
605 of Lake Erie: Central basin hypoxia”. *Journal of Great Lakes Research* 40.2, pp. 226–246.
- 606 Schwalm, C. R., Glendon, S., and Duffy, P. B. (2020). “RCP8. 5 tracks cumulative CO2 emissions”.
607 *Proceedings of the National Academy of Sciences* 117.33, pp. 19656–19657.
- 608 Sharma, S., Jackson, D. A., Minns, C. K., and Shuter, B. J. (2007). “Will northern fish populations
609 be in hot water because of climate change?” *Global Change Biology* 13.10, pp. 2052–2064.
- 610 Shi, Q. and Xue, P. (2019). “Impact of lake surface temperature variations on lake effect snow over
611 the Great Lakes region”. *Journal of Geophysical Research: Atmospheres* 124.23, pp. 12553–12567.
- 612 Subin, Z. M., Riley, W. J., and Mironov, D. (2012). “An improved lake model for climate simulations:
613 Model structure, evaluation, and sensitivity analyses in CESM1”. *Journal of Advances in*
614 *Modeling Earth Systems* 4.1.
- 615 Sun, L., Liang, X.-Z., and Xia, M. (2020). “Developing the Coupled CWRF-FVCOM Modeling
616 System to Understand and Predict Atmosphere-Watershed Interactions Over the Great Lakes
617 Region”. *Journal of Advances in Modeling Earth Systems* 12.12, e2020MS002319.
- 618 Wang, J., Bai, X., Hu, H., Clites, A., Colton, M., and Lofgren, B. (2012). “Temporal and spatial
619 variability of Great Lakes ice cover, 1973–2010”. *Journal of Climate* 25.4, pp. 1318–1329.
- 620 Wang, S., Sun, X., and Lall, U. (2017). “A hierarchical Bayesian regression model for predicting
621 summer residential electricity demand across the USA”. *Energy* 140, pp. 601–611.
- 622 Woolway, R. I. and Merchant, C. J. (2019). “Worldwide alteration of lake mixing regimes in
623 response to climate change”. *Nature Geoscience* 12.4, pp. 271–276.
- 624 Wuebbles, D., Cardinale, B., Cherkauer, K., Davidson-Arnott, R., Hellmann, J., Infante, D., and
625 Ballinger, A. (2019). “An assessment of the impacts of climate change on the Great Lakes”.
626 *Environmental Law & Policy Center.*



- 627 Xiao, C., Lofgren, B. M., Wang, J., and Chu, P. Y. (2018). “A dynamical downscaling projection of
628 future climate change in the Laurentian Great Lakes region using a coupled air-lake model”.
629 *Preprints*.
- 630 Xue, P., Eltahir, E. A., Malanotte-Rizzoli, P., and Wei, J. (2014). “Local feedback mechanisms of
631 the shallow water region around the Maritime Continent”. *Journal of Geophysical Research:
632 Oceans* 119.10, pp. 6933–6951.
- 633 Xue, P., Malanotte-Rizzoli, P., Wei, J., and Eltahir, E. A. (2020). “Coupled ocean-atmosphere
634 modeling over the Maritime Continent: A review”. *Journal of Geophysical Research: Oceans*
635 125.6, e2019JC014978.
- 636 Xue, P., Pal, J. S., Ye, X., Lenters, J. D., Huang, C., and Chu, P. Y. (2017). “Improving the
637 simulation of large lakes in regional climate modeling: Two-way lake–atmosphere coupling
638 with a 3D hydrodynamic model of the Great Lakes”. *Journal of Climate* 30.5, pp. 1605–1627.
- 639 Xue, P., Schwab, D. J., and Hu, S. (2015). “An investigation of the thermal response to meteorological
640 forcing in a hydrodynamic model of Lake Superior”. *Journal of Geophysical Research: Oceans*
641 120.7, pp. 5233–5253.
- 642 Ye, X., Anderson, E. J., Chu, P. Y., Huang, C., and Xue, P. (2019). “Impact of water mixing and ice
643 formation on the warming of Lake Superior: A model-guided mechanism study”. *Limnology
644 and Oceanography* 64.2, pp. 558–574.
- 645 Ye, X., Chu, P. Y., Anderson, E. J., Huang, C., Lang, G. A., and Xue, P. (2020). “Improved thermal
646 structure simulation and optimized sampling strategy for Lake Erie using a data assimilative
647 model”. *Journal of Great Lakes Research* 46.1, pp. 144–158.
- 648 Zhang, L., Zhao, Y., Hein-Griggs, D., Barr, L., and Ciborowski, J. J. (2019). “Projected extreme
649 temperature and precipitation of the Laurentian Great Lakes Basin”. *Global and Planetary
650 Change* 172, pp. 325–335.
- 651 Zhang, L., Zhao, Y., Hein-Griggs, D., and Ciborowski, J. J. (2018). “Projected monthly temperature
652 changes of the Great Lakes Basin”. *Environmental research* 167, pp. 453–467.
- 653 Zhang, L., Zhao, Y., Hein-Griggs, D., Janes, T., Tucker, S., and Ciborowski, J. J. (2020). “Climate
654 change projections of temperature and precipitation for the great lakes basin using the PRECIS
655 regional climate model”. *Journal of Great Lakes Research* 46.2, pp. 255–266.
- 656 Zhong, Y., Notaro, M., Vavrus, S. J., and Foster, M. J. (2016). “Recent accelerated warming of the
657 Laurentian Great Lakes: Physical drivers”. *Limnology and Oceanography* 61.5, pp. 1762–1786.